Theoretical and Applied Fracture Mechanics 95 (2018) 261–269

Contents lists available at ScienceDirect

Theoretical and Applied Fracture Mechanics

journal homepage: www.elsevier.com/locate/tafmec

Static assessment of nanoscale notched silicon beams using the averaged strain energy density method

Pasquale Gallo[a,*], Takashi Sumigawa[a], Takayuki Kitamura[a], Filippo Berto[b]

[a] Kyoto University, Department of Mechanical Engineering and Science, Kyoto-daigaku-Katsura, Nishikyo-Ku, Kyoto 615-8540, Japan
[b] Norwegian University of Science and Technology (NTNU), Department of Mechanical and Industrial Engineering, Richard Birkelands vei 2b, Trondheim, Norway

ARTICLE INFO

Keywords:
Nanoscale
Single-crystal silicon
Theory of critical distances
Strain energy density
Fracture nanomechanics

ABSTRACT

This paper extends the averaged Strain Energy Density (SED) method to the static assessment of notched components at the nanoscale. First, *in situ* micromechanical testing of notched nano-cantilever beams made of single-crystal silicon is briefly reviewed. Then, an alternative strategy based on the Theory of Critical Distances is employed to evaluate the control volume and the critical SED. The method is later verified against experiments and FE analyses. The SED method successfully estimates the load at fracture of nanoscale notched specimens with a maximum discrepancy of 4.7%. Moreover, the method is mesh-independent, and therefore very coarse meshes can be employed in numerical analyses. Finally, the results are discussed on the basis of the breakdown of continuum fracture mechanics at the nanoscale. The extension of the SED approach to the micro- and nanoscales provides a fast and simple tool for the design of micro- and nanodevices.

1. Introduction

The miniaturisation of electronic devices, for example, the use of micro- and nano-electromechanical systems (MEMS and NEMS) as sensors and actuators, have brought problems of material behaviour at the nanometer scale into the domain of fracture mechanics [1]. Thus, new challenges have arisen recently, e.g. mechanical characterisation at small scales, static and fatigue assessment at the micro and nanoscale, and development of tools for the proper design of such small components. Miniaturised devices are not free of the notches and cracks/defects encountered in their macro counterparts. However, it was unclear whether linear elastic fracture mechanics (LEFM) could be applied at small scales. Wang et al. [2] reviewed recent advances in the application of modified continuum models in nanostructures, providing a comprehensive overview of the development in that area. Recently, since *in situ* observation of mechanical behaviour at the nanoscale has advanced considerably [3–6], the questions above have sparked the interest of the scientific community. A review of a series of experimental studies at small scales was published by Sumigawa et al. [3], who showed how continuum mechanics remains applicable to fracture at the nanoscale. The concept of the plastic stress intensity factor, for example, has been used to characterise crack initiation at the interface edge at the nanoscale [7]. Huang et al. [7] demonstrated that under large-scale yield conditions, the stress distribution shows an $r^{-\lambda_P}$-type singularity, as predicted by conventional fracture mechanics. Recent studies have focused on the cracking behaviour of silicon instead [8–12]. Specifically, Sumigawa et al. [11] determined the fracture toughness in a nanoscale singular stress field of 23–58 nm by using single-crystal silicon specimens with different pre-crack lengths. The fracture toughness obtained showed good agreement with the bulk K_{IC}, proving the size independence of the fracture behaviour. Moreover, the stress distribution showed a conventional $r^{-0.5}$-type singularity, as would be expected for cracks. On the other hand, Shimada et al. [13] considered smaller scales and found that even though a singular stress field of only several nanometers still governed fracture, the stress intensity factor approach failed for stress field lengths ranging between 1.2 and 3.6 nm. Indeed, at such a small scale, one must deal with the atomic structure.

The background outlined above suggests that several tools for static and fatigue design based on LEFM and used at the macroscale may be directly scaled down to the nanoscale once the lower limit of LEFM is defined [13]. Among the standard LEFM approaches, energy-based criteria showed the potential to be easily extended beyond the dimensional limits of conventional continuum fracture mechanics. Several authors have contributed to this topic. Among them, Huang et al. [14] showed that the Griffith-based criterion describes brittle fracture of notches even below a critical size of 5 nm, below which the fracture stress fails. This result was obtained by modifying the Griffith criterion to account for the atomic discreteness at very small scales. Similarly, Sumigawa et al. [15] experimentally characterised nano-cracking

* Corresponding author.
E-mail address: pasquale.gallo@aalto.fi (P. Gallo).

https://doi.org/10.1016/j.tafmec.2018.03.007
Received 26 February 2018; Received in revised form 14 March 2018; Accepted 14 March 2018
Available online 15 March 2018

behaviour in brittle silicon and demonstrated that the classical Griffith criterion could mechanically describe nano-cracking.

While the Griffith criterion (and Energy Release Rate) has been the primary focus of much recent research (see given references), other energy approaches have been completely neglected. Among them, the averaged Strain Energy Density (SED) concept has proved to be one of the most versatile, simple, and useful tools both in fatigue and static assessment of notched components and welded joints. The method was formalised by Lazzarin and co-workers [16,17] and derived from Neuber's concept of elementary volume and the local mode I concept proposed by Erdogan and Sih [18]. The SED criterion states that failure occurs when the mean value of the SED, averaged over a control volume surrounding the notch (crack) root (tip), equals a critical value. Applications of the method are widely available in the literature for large bodies and several materials [19–27], where local inhomogeneities are neglected owing to the large volume-to-surface ratio, and recent reviews [28–30] summarise the main advantages and theoretical developments in detail. Unlike other methods, an extension of the SED approach to the micro- and nanoscales would offer enormous practical simplifications to the fatigue and static design of micro- and nanodevices. Indeed, as long as the control volume is well defined, the averaged SED method can be applied to specimens of any shape, from cracks to notches. Moreover, it would simplify Finite Element (FE) analyses thanks to its mesh-independence [16]. As explained in detail in Section 2, the control volume for static loadings is a function of the ultimate tensile stress and the fracture toughness. Gallo et al. [31] recently tried to obtain a first estimation of the averaged Strain Energy Density control volume for the static assessment of single-crystal silicon at the nanoscale. The authors proposed values of 0.84 μm and 0.99 μm for plane strain and plane stress, respectively. However, this preliminary estimation was based on an approximated tensile strength of 2 GPa. Therefore, despite the fact that the work represented a first step toward the application of the averaged SED at the nanoscale, the proposed value needed further investigation. Indeed, although the fracture toughness is fundamentally an inherent property, the yield stress is significantly affected by the specimen size [32,33], increasing as the micro- and nanoscales are approached [11]. This phenomenon is easily explained by the relationship between fracture stress and volume of the component. The fracture stress is usually studied on the assumption that fracture takes place originating from pre-existing defects or flaws. However, the defects vary in number and in severity depending on the volume (size) of the component. Ideally, the ideal fracture stress of the material having no defect is reached at the nanoscale [34]. Thus, accurate control of the final geometry and size, which is currently very challenging, plays an essential role in the determination of mechanical properties and, in turn, in the evaluation of the control volume. Compared to the application of the method at the macroscale, this is an entirely new challenge.

This paper further extends the averaged SED to the static assessment of notched components at the nanoscale by employing an alternative strategy based on the Theory of Critical Distances [35] to determine the control volume and the critical SED. The proposed procedure avoids the demanding control of the geometry at the nanoscale while obtaining accurate values for both the tensile strength and fracture toughness simultaneously, as shown in [36] for the considered scale. Moreover, it allows the introduction of the scale effect into the SED formulation within the limits of continuum fracture mechanics. Accurate FE analyses and theoretical equations yield the averaged SED, and the method is verified by reviewing *in situ* micromechanical test results for notched nano-cantilever beams available in the literature [36]. The SED criterion successfully estimates the static critical load at fracture by using both coarse and fine meshes, providing a practical tool for the static and fatigue assessment of MEMS and NEMS.

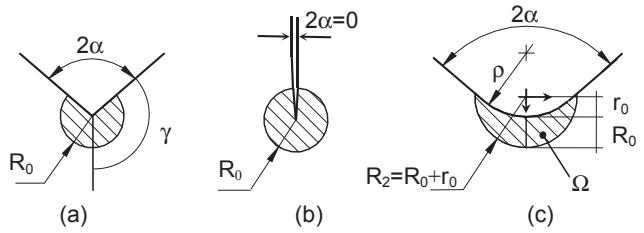

Fig. 1. Critical volume (area) for sharp V-notch (a), crack (b), and blunt V-notch (c) under mode I loading; distance $r_0 = \rho \times (\pi - 2\alpha)/(2\pi - 2\alpha)$.

2. Fundamentals of the Strain Energy Density averaged over a control volume

The averaged Strain Energy Density (SED) method was derived from Neuber's concept of elementary volume and the local mode I concept proposed by Erdogan and Sih [18]. Lazzarin and co-workers initially formalised it for notches of different geometries [16,17] and large bodies. The approach combines the concept of energy criterion with the advantages tied to the definition of a material-dependent structural volume. Some recent contributions reviewed the method in detail, including the full analytical framework and primary applications [29–31]. The approach assumes that under tensile stress, failure occurs when the strain energy density averaged over a given control volume $\overline{W}$ reaches a critical value W_c (that depends on the selected material). Fig. 1 shows an example of control volumes becoming "areas" when in-plane problems are considered. In the case of blunt notches, the area assumes a crescent shape. When mixed-mode loading is considered, the control area rotates and is aligned to the point where the principal stress reaches its maximum value [37]. The control volume R_0 depends on the fracture toughness K_{IC} and ultimate tensile stress σ_t for static loading, and on the smooth specimen fatigue limit $\Delta\sigma_0$ and the fatigue threshold ΔK_{th} (for metallic materials) for cyclic loads [38]. Under plane strain conditions, the R_0 for static loading is given by

$$R_0 = \frac{(1+\nu)(5-8\nu)}{4\pi}\left(\frac{K_{IC}}{\sigma_t}\right)^2. \tag{1}$$

Under plane stress conditions R_0 is defined as follows:

$$R_0 = \frac{(5-3\nu)}{4\pi}\left(\frac{K_{IC}}{\sigma_t}\right)^2. \tag{2}$$

The control volume/radius can also be linked to the El Haddad-Smith-Topper parameter $a_0 = (1/\pi)(K_{IC}/\sigma_t)^2$ [39] via

$$R_0 = C \cdot a_0, \tag{3}$$

where C is derived by comparing Eq. (3) to Eq. (2) (for plane stress) or Eq. (1) (for plane strain) and is a function of the Poisson's ratio alone.

If the material behaviour is ideally brittle, the critical energy value W_c can be evaluated by using the conventional ultimate tensile strength σ_t for static cases and the fatigue strength $\Delta\sigma_0$ for fatigue loading:

$$W_c = \frac{\sigma_t^2}{2E} \tag{4}$$

$$\Delta W_c = c_w \frac{\Delta\sigma_0^2}{2E} \tag{5}$$

The parameter c_w is introduced to consider the influence of the nominal load ratio on the variation of the deviatoric energy imparted to the material in one cycle [40]. It should be noted that Eqs. (1)–(5) are defined for the mode I stress distribution due to tension or bending loads. For blunt notches under static loading, the following expression can be used to determine the averaged SED analytically [17]:

$$\overline{W} = F(2\alpha) \times H\left(2\alpha, \frac{R_0}{\rho}\right) \times \frac{\sigma_{max}^2}{E}. \tag{6}$$

In Eq. (6), σ_{max} is the maximum principal stress at the notch root, E is Young's modulus, and F is a function that depends on the notch opening angle. Finally, H depends on the notch angle and the critical radius/notch tip radius ratio. Values of functions H and F for numerous Poisson's ratios and opening angles have been reported in [17,29] and are presented in Appendix A for the sake of clarity. The equation can also be expressed in a more useful form since σ_{max} can be derived as a function of the stress concentration factor K_{tn} (net section) and the applied nominal load σ_{nom}:

$$\overline{W} = F(2\alpha) \times H\left(2\alpha, \frac{R_0}{\rho}\right) \times \frac{(\sigma_{nom} \cdot K_{tn})^2}{E}. \tag{7}$$

In the case of sharp notches, the Mode I notch stress intensity factor K_I^V is introduced and the following equation is employed:

$$\overline{W} = \frac{I_1}{4E\lambda_1\gamma}\left(\frac{K_I^V}{R_0^{1-\lambda_1}}\right), \tag{8}$$

where λ_1 is the Williams' eigenvalue while $\gamma = \pi - \alpha$ depends on the notch opening angle 2α. Parameter I_1 is tabulated in Table A3 for different values of the Poisson's ratio. Further details on Eq. (8) can be found in [29] and are omitted here since sharp notches are not considered in the present paper.

Once the control volume is defined, the SED can be evaluated through the above equations for the geometry of interest, or by more practical FE analysis. Indeed, the mean value of the elastic SED on the control volume can be determined with high accuracy by using very coarse meshes [41]. The SED is derived from the numerical nodal displacements, which are not affected by the mesh refinement. Provided that all the material inhomogeneities can be averaged, the SED approach has proven to be a powerful tool both for static and fatigue strength assessment of notched components.

3. Validation of the averaged SED at the nanoscale

3.1. Evaluation of the control volume

The control volume for static loadings, as introduced in the previous section, is a function of the ultimate tensile stress and the fracture toughness. Gallo et al. [31] recently provided a first estimation of the averaged SED control volume at the nanoscale for single-crystal silicon. They proposed a value of 0.84 μm for plane strain. However, this preliminary estimation was based on Eq. (1) and on approximated values of the tensile strength (2 GPa) and fracture toughness (1 MPa·m$^{0.5}$). Although the fracture toughness is fundamentally inherent, the yield stress is significantly affected by the material size [32,33], increasing as the micro- and nanoscales are approached [11]. Thus, the control volume was affected by the tensile strength chosen and was not valid for different specimen sizes. In other words, the scale effect was not appropriately considered. However, an alternative procedure based on the theory of critical distances (TCD) [42] enables rapid evaluation of the control volume for the considered scale. According to the TCD, failure occurs when the principal stress σ_1 at a given distance $L/2$ from the notch tip reaches the inherent material strength σ_0. L, the so-called characteristic length, is considered to be a material property and is defined as [35]

$$L = \frac{1}{\pi}\left(\frac{K_{IC}}{\sigma_0}\right)^2. \tag{9}$$

At the nanoscale, the inherent material strength σ_0 can be considered to be the ideal fracture stress, i.e. the upper limit of fracture stress of components having no defect. This limit, once reached, should not be affected by further changes in the size of the specimen and can be correlated to the atomic level mechanisms [34].

By combining Eq. (9) with the definitions in Eqs. (1) and (2), it is possible to define the control volume as a function of L through the El Haddad-Smith-Topper parameter [39] introduced earlier in Eq. (3). Indeed, $L = a_0 = (1/\pi)(K_{IC}/\sigma_t)^2$ and therefore:

$$R_0 = \frac{(1+\nu)(5-8\nu)}{4}\frac{1}{\pi}\left(\frac{K_{IC}}{\sigma_t}\right)^2 = \frac{(1+\nu)(5-8\nu)}{4}L \quad \text{(for plane strain)}, \tag{10}$$

$$R_0 = \frac{(5-3\nu)}{4}\frac{1}{\pi}\left(\frac{K_{IC}}{\sigma_t}\right)^2 = \frac{(5-3\nu)}{4}L \quad \text{(for plane stress)}. \tag{11}$$

It should be noted that when the characteristic length L is defined for the specimens (and their scale), the control volume is automatically defined without any assumptions about the other mechanical properties. According to the comments provided earlier, for brittle materials, the TCD inherent material stress σ_0 is representative of the ideal fracture stress, i.e. the limit of a component having no defects. Therefore, the critical SED at failure can be redefined as follows:

$$W_c = \frac{\sigma_0^2}{2E}. \tag{12}$$

Gallo et al. [36] recently evaluated the characteristic length for single-crystal silicon under static loads. They investigated the nanoscale fracture behaviour of silicon and showed that the TCD could correctly estimate the fracture toughness at the nanoscale. *In situ* micromechanical testing of notched nano-cantilever beams was carried out in a transmission electron microscope (TEM). Four specimens were fabricated by a focused ion beam (FIB) processing system with notch radii of 10.2, 6.3, 20.2, and 13.8 nm and opening angles 2α of 33°, 68°, 59°, and 48° respectively. Details on the specimen fabrication process and all the geometrical parameters have been reported in [36], and Fig. 2 presents an example of the final sample. The above geometries gave stress concentration factors K_{tn} (net section) of 4.3, 4.9, 2.9, and 3.7, respectively [36].

The specimens were later loaded into the TEM using a sample holder with a loading device. The TEM was equipped with an *in situ* observation camera, and the loading device consisted of a stage capable of being moved freely to achieve correct alignment. The load was applied to the specimens by pushing onto the indenter while the load was detected by a sensor beneath the indenter. The deflection at failure δ_f and load at failure P_f were obtained. The results are summarized in Table 1 together with main geometrical parameters of the notches (refer to Fig. 3); details can be found in [36]. Following the definition by Susmel et al. [43,44] and Taylor et al. [35,42], fracture toughness K_{IC} and the material characteristic length L were determined by overlapping on a single graph the linear elastic stress fields of the considered notches under incipient failure conditions. The average value of the fracture toughness was 0.98 MPa·m$^{0.5}$, while L varied between 1.3 and 1.9 nm (i.e., 1.6 nm on average). The inherent material strength σ_0 was 13.9 GPa.

By using Eq. (10), the averaged SED control volume R_0 for plane strain conditions is found to be 1.4 nm. This value is calculated by assuming a Poisson's ratio and Young's modulus of 0.28 and 130 GPa [45], respectively, for the [1 0 0] crystal plane, as reported in [36].

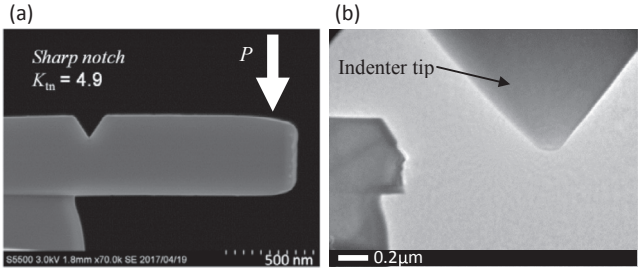

Fig. 2. Example of (a) nanoscale notched specimen tested in [36] (SEM image), and TEM image of the sample after final failure (b).

Table 1
Main geometrical parameters of notches (see Fig. 3), final deflections to failure, and loads at fracture of the nano-cantilever notches; details can be found in [36].

Specimen	2α (deg)	a (nm)	d (nm)	ρ (nm)	K_{tn}	δ_f (nm)	P_f (μN)
1	33	155	217	10.2	4.3	99.96	45.33
2	68	144	87	6.3	4.9	83.74	30.84
3	59	179	119	20.2	2.9	115.59	65.11
4	48	161	96	13.8	3.7	83.59	84.80

Through Eq. (12), the critical SED redefined by the inherent material stress σ_0 of the TCD is calculated to be 0.7431 GJ/m^3. These values are later verified against data from [36] and finite element analyses.

3.2. FE analyses

The micromechanical tests presented in [36] and briefly reviewed in Section 3.1 were re-analysed by using the control volume evaluated in the previous section. Nano-cantilevers were modelled by using the *Ansys® Apdl 15.0* finite element software package, and linear elastic analyses were conducted. The model consists of a notched nano-cantilever beam and relative block derived from the fabrication process. Fig. 3 shows the simplified geometry of a typical sample. The block is assumed to be ten times bigger than the cantilever and fully constrained along its lower and lateral surfaces, as depicted in Fig. 3. Plane strain conditions were assumed and, given the condition of in-plane loading, a 2D 8-node element-type PLANE183 [46] with unit thickness was employed. The anisotropy of the single-crystal silicon was defined by the three material constants [11] reported in Fig. 3, *viz.*, C_{11} = 167.4 GPa, C_{22} = 65.23 GPa, and C_{44} = 79.57 GPa. The load was applied at the end of the cantilever following the configurations and loads reported in [36] (see Table 1). Coarse and accurate meshes were realised to verify the mesh independence of the SED at the nanoscale. Two procedures were followed:

i. First, the experimental loads reported in Table 1 were applied to the models; then, the averaged SED was determined over a control volume of 1.4 nm. The aim was to verify the constancy of the averaged SED at incipient failure and to compare this value to the theoretical critical strain energy density modified by the TCD of Eq. (12), i.e. 0.7431 GJ/m^3. This step was necessary to verify the main assumption of the SED method, i.e., that failure occurs when the SED over a control volume reaches a critical value. The results were also compared to the analytical formulation, i.e. Eq. (7).
ii. Upon verification of (i), the theoretical critical SED (0.7431 GJ/m^3) was assumed as input parameter instead, and the respective loads were evaluated a posteriori only for the cases that showed the highest percentage difference in (i). These values were then compared to the experimental loads in Table 1. The aim was to highlight the effect of the scatter/discrepancy between the experimental averaged SED at failure and Eq. (12) on the determination of the load at failure.

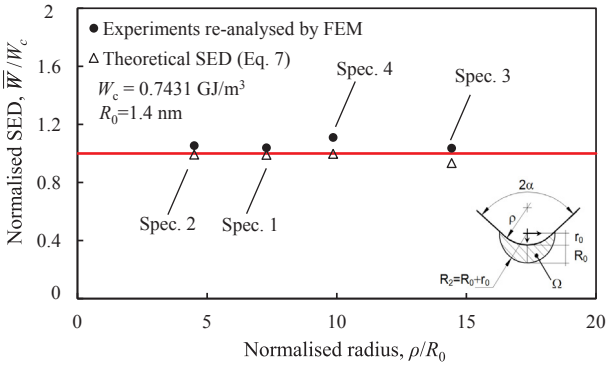

Fig. 4. Static failure data in terms of normalised strain energy density.

4. Results

4.1. Static assessment through the averaged SED approach

Fig. 4 compares the normalised SED at failure evaluated by FE analyses and by Eq. (7) to the critical SED of Eq. (12). The FE analysis results show excellent agreement, which proves that the SED averaged over the proposed control volume can predict the load at failure reported in [36]. All values are well aligned with the theoretical critical SED modified with the TCD inherent strength, i.e., Eq. (12). The scatter is minimal, and it is mainly due to the unavoidable uncertainty in the definition and measurement of the geometry in [36]. More comments are provided in the discussion in Section 5. Surprisingly, also the theoretical averaged SED, as defined by Eq. (7), shows excellent agreement with critical SED and FE results. Indeed, for all the specimens, the normalised SED ratio is very close to the theoretical value of 1. However, specimen 3 shows a slight deviation. This can be easily explained. Parameters F and H were provided in [29] for limited opening angles and Poisson's ratios; the geometries under consideration in the present paper were not included. Thus, the present authors derived these parameters by linear interpolation on the basis of the values reported in Tables A1 and A2 in the Appendix, for a Poisson's ratio ν of 0.3. The approximations made during the derivation lead to unavoidable but minimal discrepancies. Even with these approximations, the results are excellent. For the sake of clarity, the FE analysis results are summarised in Table 2, while Table 3 lists the parameters employed in Eq. (7) and the theoretical SED values. The σ_{nom} is the maximum bending stress according to the Euler-Bernoulli beam bending theory for the geometry presented in [36].

Clearly, the difference between the experimental SED at failure and the critical SED W_c is negligible for all specimens. In Table 2, the percentage difference is minimal for specimens 1, 2, and 3, reaching a maximum of 10% for specimen 4. However, these differences are expected to be reduced when the nominal loads at failure are evaluated because of the mathematical relationship between stresses and SED. As an example, let us consider specimen 4, which exhibits the highest discrepancy. By following the procedure engineers would follow in practical applications for determining the load at fracture, the W_c value of 0.7431 GJ/m^3 is assumed as a reference, and the external load is then

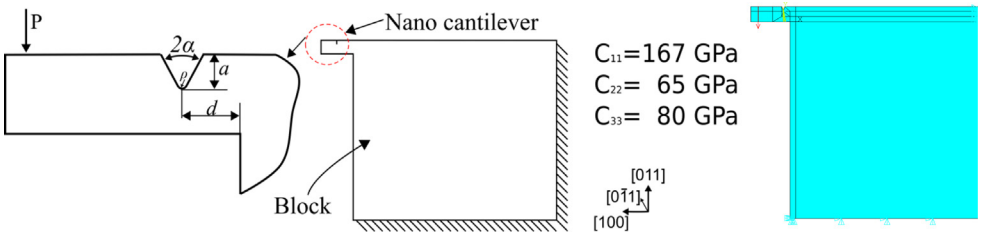

Fig. 3. Schematics of the block, nano-specimens, and material constants (left), and FE model (right).

Table 2
Static failure data in terms of strain energy density and percentage difference between FE analyses and critical SED of Eq. (12).

Spec.	R_0 (nm)	2α (deg)	r_0 (nm)	$\overline{W}$ (GJ/m^3)	W_c (GJ/m^3)	Δ%
1	1.4	33	4.59	0.7720	0.7431	4%
2	1.4	68	2.42	0.7830	0.7431	5%
3	1.4	59	8.12	0.7700	0.7431	4%
4	1.4	48	5.84	0.8249	0.7431	10%

Table 3
Theoretical SED obtained from Eq. (7) and parameters H, and F.

Spec.	R_0/ρ	2α (deg)	H	$F(2\alpha)$	σ_{nom} (GPa)	E (GPa)	$\overline{W}$ (GJ/m^3)
1	0.1	33	0.5107	0.6917	3.83	130	0.7359
2	0.2	68	0.4425	0.6720	3.66	130	0.7262
3	0.07	59	0.5850	0.6620	5.26	130	0.6937
4	0.1	48	0.5204	0.6760	4.47	130	0.7408

determined by FE analysis, by using the same model as in Section 3.2. The results show that W_c is generated by an external load P of 80.9 μN, while the experiments (see Table 1) give a load at fracture P_f of 84.80 μN. The percentage difference between these two values is only 4.7% and within safety limits since the load is slightly underestimated.

4.2. Mesh independence

Different meshes have been used in the FE simulations described in Section 3.2. Fig. 5 shows an example of the mesh refinement levels of specimen 1's control volume. Others models are omitted for the sake of brevity since they are very similar. Essential details on all models are given in Tables 4–7. These include the number of elements used to model the control volume, the averaged SED, and the percentage difference between coarse meshes and the reference fine mesh. The tables show that all the meshes yield an accurate estimation of the averaged SED over the control volume (area) for all specimens, regardless of the notch radius and/or opening angle. The maximum difference between models with very refined and coarse meshes is 1.1% (Table 6, specimen 3) and thus negligible. It is well known that other approaches based on stresses or stress intensity factors are highly mesh-sensitive. The SED approach offers a significant advantage over these other approaches, enabling rapid calculation with very simple and coarse meshes.

The mesh insensitivity of the averaged SED is easily explained by considering the theoretical basis of the FE method: The strain energy is determined numerically from nodal displacements, without any calculation of stresses and strains. Consequently, the degree of accuracy depends only on the element type, i.e., the shape function. On the other hand, the numerical evaluation of stresses involves derivation and/or integration processes that vary significantly with mesh size [47].

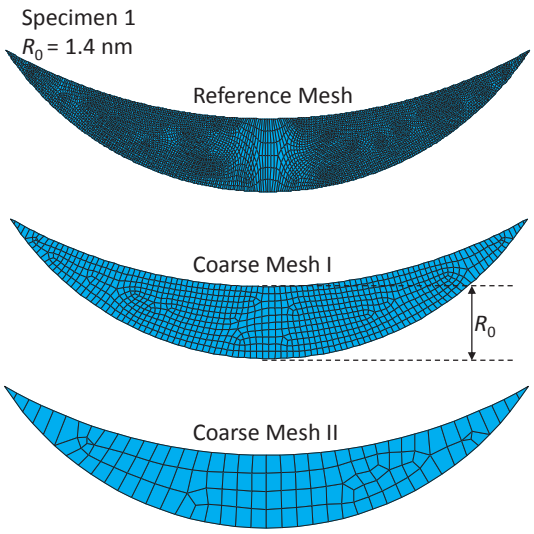

Fig. 5. Control volume of specimen 1 FE model for different mesh refinements.

Table 4
Averaged values of the SED of specimen 1 for different mesh refinements.

Specimen 1	Number of FEs in R_0	$\overline{W}$ (GJ/m^3)	Δ%
Reference Mesh	15,211	0.7720	–
Coarse Mesh I	795	0.7721	0
Coarse Mesh II	117	0.7798	1

Table 5
Averaged values of the SED of specimen 2 for different mesh refinements.

Specimen 2	Number of FEs in R_0	$\overline{W}$ (GJ/m^3)	Δ%
Reference Mesh	14,732	0.7830	–
Coarse Mesh I	636	0.7799	0.4
Coarse Mesh II	94	0.7821	0.1

Table 6
Averaged values of the SED of specimen 3 for different mesh refinements.

Specimen 3	Number of FEs in R_0	$\overline{W}$ (GJ/m^3)	Δ%
Reference Mesh	16,835	0.7700	–
Coarse Mesh I	891	0.7712	0.2
Coarse Mesh II	112	0.7789	1.1

Table 7
Averaged values of the SED of specimen 4 for different mesh refinements.

Specimen 4	Number of FEs in R_0	$\overline{W}$ (GJ/m^3)	Δ%
Reference Mesh	15,839	0.8249	–
Coarse Mesh I	734	0.8198	0.6
Coarse Mesh II	89	0.8317	0.8

5. Discussion

Micro- and nanosize components invariably present experimental difficulties, in particular, during mechanical characterization. These difficulties arise because the realization of an accurate geometry becomes problematic at very small scales, while, at the same time, it also becomes critically important. Even when the mechanical properties are defined, size dependence plays a fundamental role and cannot be neglected, unlike in large bodies and macro components. This is exemplified by the fracture toughness of single-crystal silicon. Ando et al. [8] and Li et al. [9] found that the K_{IC} of nano-Si was in some cases twice as large as its macro counterpart. Sumigawa et al. [11] found that such discrepancies were due to the small radius of the crack tip, which had a significant effect on the final fracture toughness value. Sumigawa et al. [11] then conducted mechanical tests on pre-cracked samples, making sure that an effective crack tip was realized. The results yielded a nano-Si K_{IC} of 1 MPa·m$^{0.5}$, in agreement with the macro scale [11]. The application of any method for design or characterization at the nano- and microscales involves the definitions of the mechanical properties; thus, all the difficulties and uncertainties reported above apply. The SED approach seems to present the very same problems in terms of the definitions of the control volume and the critical SED. However, the present study showed that some difficulties can be overcome by exploiting the TCD, which brings two main advantages: (i) it eliminates the need for strict control of the geometry (i.e., K_{IC} is

derived by using notches of generic "different sharpnesses"); (ii) the fracture toughness and the so-called inherent material strength are defined simultaneously. These benefits also affect the SED method once the TCD is introduced into its formulation by modifying W_c, as shown in Eq. (12), and by determining the control volume as a function of the material characteristic length L. With this strategy, the main parameters of the SED, i.e., R_0 and W_c, are completely defined and can be easily employed for static assessment. The results showed that by employing a control volume of 1.4 nm, the method gives an excellent estimation of the load at fracture. Indeed, all specimens showed an averaged SED at failure very close to W_c (see Fig. 4). The maximum discrepancy was 10% in terms of SED (specimen 4 in Table 2), which corresponds to 4.7% in terms of load.

The control volume proposed in the present paper, 1.4 nm, is considerably smaller than the value given previously in [31], 0.84 μm. However, this does not invalidate either value. Indeed, the difference may be explained by considering a significant factor: the specimen size (scale). Bulk components have indeed a large volume which contains a large number of small cracks (defects), and therefore the fracture stress decreases. On the other hand, as the component size goes down, the volume, the number of small cracks and the maximum defect size (that governs the fracture stress) also decreases. At very small scales (such as nanoscale components), there is ideally no crack/defects in the considered volume, and the ideal strength σ_0 is reached. At this point, σ_0 should not be affected by further changes in the specimen size, and it can be related to the atomic level interactions [34]. In [31] the specimens were larger and the ultimate tensile strenght value of 2 GPa was only an estimation. This parameter, as shown in Eqs. (1) and (2), dramatically changes the control volume. The same consideration is valid for the fracture toughness. Indeed, it is shown that K_{IC} is inherent in the case of single-crystal silicon, but this property has yet to be proved for other materials. In contrast to the macroscale, where the control volume depends only on the mechanical properties, the scale and size of the specimen affect the control volume as an additional variable. The solution proposed in the present work aims to correlate the control volume to the scale effect by the TCD. The TCD lies between continuum mechanics theories and micro-mechanistic approaches, which attempt to model the physical mechanics of the fracture/failure at very small scales. The material characteristic length L can be considered to be a representative length scale parameter that assumes different values as the micromechanisms of fracture change scale [48], while σ_0 is representative of the ideal fracture stress on the basis of the relationship between fracture stress and component volume. Even though these considerations seem in contrast with the definition of L as a "material property", Taylor [42] extensively showed how the TCD is capable of predicting the size effect, and how, for smaller scales on the order of L, the latter may become a variable quantity [49]. Therefore, when these two parameters are introduced into the theoretical formulation of the SED, as shown in Section 3.1, the critical SED and the control volume are implicitly modified to take into account the scale effect. First, the critical SED is redefined through the TCD inherent material strength σ_0, which is representative of the specimens (and scale) being considered. By so doing, any uncertainty in the assumption of static strength is overcome. Subsequently, the control volume is defined in terms of L and thus may vary with L and the micromechanisms involved in the fracture process. The excellent results obtained here demonstrate that the combination of the two approaches is a winning choice.

Surprisingly, the excellent agreement is not limited to the SED evaluated through FE analysis but is also valid for its theoretical formulation, i.e. Eq. (7), as shown in Fig. 4. All the normalised SED ratios are very close to the theoretical value of 1. The small scatter is clearly due to approximations in the parameters F and H. These were provided in [29] for limited geometries, and have thus been derived in the present work by linear interpolation on the basis of the values reported in the Appendix (refer to $\nu = 0.3$). These approximations are reasonable, but a better estimation (left for future work) should include new definitions for F and H, by following the procedure reported in [29]. It is more interesting instead to dwell on the fact that the theoretical formulation presented in Section 2 was developed for large bodies (large volume-to-surface ratio) and continuum models. Clearly, those assumptions become questionable as the micro and nanoscales are approached. However, the theoretical formulation of the SED (see Fig. 4) still gives excellent results when applied to the nano-cantilevers considered here [36]. This can be explained by taking into account the low limit of continuum fracture mechanics and the scale at which Si micromechanisms of fracture occur. Sumigawa et al. [15] analyzed single-crystal Si at the atomic level by using density functional theory (DFT) calculations and showed that the initiation of nano-cracking is dominated by the cleavage of atomic bonds at the crack tip, and thus occurs at smaller scales than the one considered in the present paper. These micromechanisms govern not only the fracture of Si at small scales but at the macroscale as well. It seems, therefore, that the control volume proposed in the present work is still representative of the fracture process, despite the scale effect. Shimada et al. [13] evaluated the ultimate dimensional limit of fracture mechanics at the nanoscale by considering only several atoms in a singular stress field of several nanometers near a crack tip. They found that the singular stress field still governed the fracture, but classic approaches such as those involving the stress intensity factor failed below a specific length scale. On the basis of classical atomic simulations and first-principles density-functional theory calculations, Shimada et al. [13] identified a *fracture process zone* Λ_f of 0.4–0.6 nm, and a *stress intensity factor dominant region* Λ_k of 1.2–3.6 nm. For values of the singular stress field close to the lower limit of Λ_k, continuum fracture mechanics breaks down. While the relationship between these values and the TCD material characteristic length has already been addressed in the recent literature [36], the results of the present paper lead to a further discussion that also considers the SED control volume. Interestingly, the control volume $R_0 = 1.4$ nm falls within the range of Λ_k, and, more importantly, it is larger than and contains the fracture process zone. It is thus demonstrated that the control volume employed in the present work is representative of the micromechanisms of fracture and yet still falls within the range of validity of continuum fracture mechanics. If the high level of homogeneity of single-crystal Si is considered as well, it is possible to conclude that the central assumptions of the SED theory are verified. In other words, once the lower limit of continuum fracture mechanics is identified and until that limit is reached effectively, the SED method remains valid, provided that the control volume and critical SED are calibrated correctly. Indeed, even though the lower limit of continuum theory is not reached, a scale effect still clearly exists, and parameters become variable quantities. By contrast, at smaller scales, continuum mechanics fails and one must deal with atomic structure. In this case, energy criterions seem more flexible than others in adapting to discrete models [13–15].

In the present work, the SED has been combined with the TCD. For the sake of clarity, it should be pointed out that Berto at al. [50] proposed an additional method to determine the control volume. In [50], brittle fracture of sharp and blunt V-notches in isostatic graphite under pure compression loading was investigated by using the averaged SED criterion. Because of the impossibility of defining the fracture toughness under a compressive load, the equations presented in Section 2 could not be used to derive critical SED and control volume. Therefore, Berto at al. [50] employed an empirical approach. Similarly to the TCD procedure in determining the critical length, the SED of at least two notches having different sharpnesses were plotted in the same graph by varying the control volume. The critical SED and the final control volume were defined by the point at which the two curves crossed over. This empirical procedure showed excellent results [50], but it did not give information on other mechanical properties and micromechanics of fracture. Lastly, it involved additional FEM models. By the way, since the present paper has finally given proves of the validity of the SED at the nanoscale and defined the length scale of the control volume,

nothing prohibits to apply this alternative procedure in the future.

The SED approach has been applied here to static loads. Given the excellent results and essential properties such as mesh-insensitivity, a further extension to fatigue loads at small scales may have a relevant technological impact. Moreover, it could be interesting to extend others well-known fracture models to micro- and nanoscale, e.g. cohesive crack model [51,52], and finite fracture mechanics (FFM) [53–55] which has many similarities with the TCD.

6. Conclusion

This study extended the averaged Strain Energy Density (SED) method to the static assessment of notched components at the nanoscale. An alternative strategy based on the Theory of Critical Distances is employed to evaluate the correct SED control volume and critical SED. The method is later verified against experiments [36] and FE analyses. The following conclusions can be drawn:

- The theoretical critical SED is redefined by using the ideal fracture stress (the limit of components having no defects) σ_0 provided by the TCD; this solution allows the critical SED to be correlated implicitly to the size of the component.
- The control volume is evaluated by using the TCD characteristic length evaluated in [36] and the El Haddad-Smith-Topper parameter [39].
- The control volume proposed is 1.4 nm (plane strain), while the critical SED is 0.7431 GJ/m^3.
- The SED averaged over the control volume obtained by using the TCD successfully estimates the static load at fracture of nanoscale notched specimens; the maximum discrepancy is found to be 4.7% in terms of load and 10% in terms of SED.
- The theoretical SED also yields excellent results, and the normalised SED ratio is close to the theoretical value of 1; the small discrepancies are undoubtedly due to the use of approximated values for the parameters H and F.
- The method is mesh-independent, and therefore very coarse meshes can be employed in numerical analyses.
- The extension of the SED approach at the micro- and nanoscales provides a fast and simple tool for the design of micro- and nanodevices since it can be applied easily to various geometries, from cracks to notches.
- It is shown that, within the limits of continuum fracture mechanics, LEFM approaches such as the SED can be easily scaled down to the nanoscale, provided that the main parameters (that become variables) are calibrated to take into account the scale effect.

Acknowledgments

The authors are grateful to the Japan Society for the Promotion of Science (JSPS) for supporting the present work (Grant-in-Aid for JSPS Fellows No. 16F16366).

Appendix A

A.1. SED method for static loading: Fundamental equations and parameters list

In the case of static loading, the critical strain energy density can be expressed as [16,28,29]:

$$W_c = \frac{\sigma_t^2}{2E} \tag{A.1}$$

The control volume, over which the strain energy density is being averaged, is a function of certain mechanical properties:

$$R_0 = \frac{(1+\nu)(5-8\nu)}{4\pi}\left(\frac{K_{IC}}{\sigma_t}\right)^2 \quad \text{(plane strain)} \tag{A.2}$$

$$R_0 = \frac{(5-3\nu)}{4\pi}\left(\frac{K_{IC}}{\sigma_t}\right)^2 \text{(plane stress)} \tag{A.3}$$

In the case of sharp and blunt V-notches, the averaged strain energy density can be obtained from Eqs. (A.4) and (A.5). Necessary material properties are given in Tables A.1–A.3, and can also be found in Refs. [28,29].

$$\overline{W_1} = \frac{I_1}{4E\lambda_1(\pi-\alpha)}\left(\frac{K_1}{R_0^{1-\lambda_1}}\right)^2 \quad \text{(sharp V-notches)} \tag{A.4}$$

$$\overline{W_1} = F(2\alpha) \times H\left(2\alpha, \frac{R_0}{\rho}\right) \times \frac{K_{tn}^2 \sigma_{nom}^2}{E}, \quad \text{(blunt V-notches)} \tag{A.5}$$

Table A1
Parameter $F(2\alpha)$ [29].

2α (rad)	$F(2\alpha)$
0	0.7850
$\pi/6$	0.6917
$\pi/4$	0.6692
$\pi/3$	0.6620
$\pi/2$	0.7049
$2\pi/3$	0.8779
$3\pi/4$	1.0717
$5\pi/6$	1.4417

Table A2
Values of function H for blunted V-shaped notches [17,29].

		H					H		
2α (rad)	R_0/ρ	ν = 0.3	ν = 0.35	ν = 0.4	2α (rad)	R_0/ρ	ν = 0.3	ν = 0.35	ν = 0.4
0	0.01	0.5638	0.5432	0.5194	π/2	0.01	0.6290	0.6063	0.5801
	0.05	0.5086	0.4884	0.4652		0.05	0.5627	0.5415	0.5172
	0.1	0.4518	0.4322	0.4099		0.1	0.4955	0.4759	0.4535
	0.3	0.3069	0.2902	0.2713		0.3	0.3296	0.3144	0.2972
	0.5	0.2276	0.2135	0.1976		0.5	0.2361	0.2246	0.2115
	1	0.1314	0.1217	0.1110		1	0.1328	0.1256	0.1174
π/6	0.01	0.6395	0.6162	0.5894	2π/3	0.01	0.5017	0.4836	0.4628
	0.05	0.5760	0.5537	0.5280		0.05	0.4465	0.4298	0.4106
	0.1	0.5107	0.4894	0.4651		0.1	0.3920	0.3767	0.3591
	0.3	0.3439	0.3264	0.3066		0.3	0.2578	0.2467	0.2339
	0.5	0.2531	0.2386	0.2223		0.5	0.1851	0.1769	0.1676
	1	0.1428	0.1333	0.1226		1	0.1135	0.1079	0.1015
π/3	0.01	0.6678	0.6436	0.6157	3π/4	0.01	0.4114	0.3966	0.3795
	0.05	0.5998	0.5769	0.5506		0.05	0.3652	0.3516	0.3359
	0.1	0.5302	0.5087	0.4842		0.1	0.3206	0.3082	0.2938
	0.3	0.3543	0.3372	0.3179		0.3	0.2082	0.1997	0.1900
	0.5	0.2597	0.2457	0.2301		0.5	0.1572	0.1504	0.1427
	1	0.1435	0.1349	0.1252		1	0.1037	0.0988	0.0932

Table A3
Parameter I_1 for sharp, zero-radius V-notches (plane strain) [29].

			I_1						
2α (degrees)	γ/π (rad)	λ_1	ν = 0.10	ν = 0.15	ν = 0.2	ν = 0.25	ν = 0.3	ν = 0.35	ν = 0.4
0	1	0.5000	1.1550	1.0925	1.0200	0.9375	0.8450	0.7425	0.6300
15	23/24	0.5002	1.1497	1.0880	1.0162	0.9346	0.8431	0.7416	0.6303
30	11/12	0.5014	1.1335	1.0738	1.0044	0.9254	0.8366	0.7382	0.6301
45	7/8	0.5050	1.1063	1.0499	0.9841	0.9090	0.8247	0.7311	0.6282
60	5/6	0.5122	1.0678	1.0156	0.9547	0.8850	0.8066	0.7194	0.6235
90	3/4	0.5445	0.9582	0.9173	0.8690	0.8134	0.7504	0.6801	0.6024
120	2/3	0.6157	0.8137	0.7859	0.7524	0.7134	0.6687	0.6184	0.5624
135	5/8	0.6736	0.7343	0.7129	0.6867	0.6558	0.6201	0.5796	0.5344
150	7/12	0.7520	0.6536	0.6380	0.6186	0.5952	0.5678	0.5366	0.5013

References

[1] T. Kitamura, T. Sumigawa, H. Hirakata, T. Shimada, Fracture Nanomechanics, 2nd ed., Pan Stanford Publishing, Singapore, 2016.
[2] K.F. Wang, B.L. Wang, T. Kitamura, A review on the application of modified continuum models in modeling and simulation of nanostructures, Acta Mech. Sin. 32 (2016) 83–100, http://dx.doi.org/10.1007/s10409-015-0508-4.
[3] T. Sumigawa, H. Fang, E. Kawai, T. Kitamura, Mechanics of fracture in nanometer-scale components, Mech. Eng. Rev. 1 (2014), http://dx.doi.org/10.1299/mer.2014smm0007 SMM0007-SMM0007.
[4] S.W. Cho, I. Chasiotis, Elastic properties and representative volume element of polycrystalline silicon for MEMS, Exp. Mech. 47 (2007) 37–49, http://dx.doi.org/10.1007/s11340-006-0405-7.
[5] M.A. Haque, M.T.A. Saif, A review of MEMS-based microscale and nanoscale tensile and bending testing, Exp. Mech. 43 (2003) 248–255, http://dx.doi.org/10.1177/0014485103036018.
[6] T. Sumigawa, T. Kitamura, In-situ mechanical testing of nano-component in TEM, in: K. Maaz (Ed.), Transm. Electron Microsc. InTech, 2012, pp. 355–380 http://www.intechopen.com/books/the-transmission-electron-microscope/in-situ-mechanical-testing-of-.
[7] K. Huang, Y. Yan, T. Sumigawa, L. Guo, T. Kitamura, Crack initiation at interface edge by nanometer scale plastic stress intensity, Eng. Fract. Mech. 178 (2017) 392–400, http://dx.doi.org/10.1016/j.engfracmech.2017.03.004.
[8] T. Ando, X. Li, S. Nakao, T. Kasai, H. Tanaka, M. Shikida, K. Sato, Fracture toughness measurement of thin-film silicon, Fatigue Fract. Eng. Mater. Struct. 28 (2005) 687–694, http://dx.doi.org/10.1111/j.1460-2695.2005.00920.x.
[9] X. Li, T. Kasai, S. Nakao, H. Tanaka, T. Ando, M. Shikida, K. Sato, Measurement for fracture toughness of single crystal silicon film with tensile test, Sens. Actuat. A Phys. 119 (2005) 229–235, http://dx.doi.org/10.1016/j.sna.2003.10.063.
[10] K. Yasutake, M. Iwata, K. Yoshii, M. Umeno, H. Kawabe, Crack healing and fracture strength of silicon crystals, J. Mater. Sci. 21 (1986) 2185–2192, http://dx.doi.org/10.1007/BF00547968.
[11] T. Sumigawa, S. Ashida, S. Tanaka, K. Sanada, T. Kitamura, Fracture toughness of silicon in nanometer-scale singular stress field, Eng. Fract. Mech. 150 (2015) 161–167, http://dx.doi.org/10.1016/j.engfracmech.2015.05.054.
[12] D. Holland, M. Marder, Ideal brittle fracture of silicon studied with molecular dynamics, Phys. Rev. Lett. 80 (1998) 746–749, http://dx.doi.org/10.1103/PhysRevLett. 80.746.
[13] T. Shimada, K. Ouchi, Y. Chihara, T. Kitamura, Breakdown of continuum fracture mechanics at the nanoscale, Sci. Rep. 5 (2015) 8596, http://dx.doi.org/10.1038/srep08596.
[14] K. Huang, T. Shimada, N. Ozaki, Y. Hagiwara, T. Sumigawa, L. Guo, T. Kitamura, A unified and universal Griffith-based criterion for brittle fracture, Int. J. Solids Struct. 128 (2017) 67–72, http://dx.doi.org/10.1016/j.ijsolstr.2017.08.018.
[15] T. Sumigawa, T. Shimada, S. Tanaka, H. Unno, N. Ozaki, S. Ashida, T. Kitamura, Griffith criterion for nanoscale stress singularity in brittle silicon, ACS Nano. 11 (2017) 6271–6276, http://dx.doi.org/10.1021/acsnano.7b02493.
[16] P. Lazzarin, R. Zambardi, A finite-volume-energy based approach to predict the static and fatigue behavior of components with sharp V-shaped notches, Int. J. Fract. 112 (2001) 275–298, http://dx.doi.org/10.1023/A:1013595930617.
[17] P. Lazzarin, F. Berto, Some expressions for the strain energy in a finite volume surrounding the root of blunt V-notches, Int. J. Fract. 135 (2005) 161–185, http://dx.doi.org/10.1007/s10704-005-3943-6.
[18] F. Erdogan, G.C. Sih, On the crack extension in plates under plane loading and transverse shear, J. Basic Eng. 85 (1963) 519–525, http://dx.doi.org/10.1115/1.3656897.
[19] M.R. Ayatollahi, F. Berto, A. Campagnolo, P. Gallo, K. Tang, Review of local strain energy density theory for the fracture assessment of V-notches under mixed mode loading, Eng. Solid Mech. 5 (2017) 113–132, http://dx.doi.org/10.5267/j.esm.2017.3.001.
[20] P. Gallo, F. Berto, Advanced materials for applications at high temperature: fatigue assessment by means of local strain energy density, Adv. Eng. Mater. 18 (2016) 2010–2017, http://dx.doi.org/10.1002/adem.201500547.
[21] P. Gallo, F. Berto, G. Glinka, Analysis of creep stresses and strains around sharp and blunt V-notches, Theor. Appl. Fract. Mech. 85 (2016) 435–446, http://dx.doi.org/10.1016/j.tafmec.2016.06.003.
[22] F. Berto, P. Gallo, Extension of linear elastic strain energy density approach to high temperature fatigue and a synthesis of Cu-Be alloy experimental tests, Eng. Solid Mech. 3 (2015) 111–116, http://dx.doi.org/10.5267/j.esm.2015.1.004.
[23] P. Gallo, F. Berto, High temperature fatigue tests and crack growth in 40CrMoV13.9 notched components, Frat. Ed Integrita Strutt. 9 (2015) 180–189, http://dx.doi.

org/10.3221/IGF-ESIS.34.19.
[24] A. Torabi, F. Berto, Strain energy density to assess mode II fracture in U-notched disk-type graphite plates, Int. J. Damage Mech. 23 (2014) 917–930, http://dx.doi.org/10.1177/1056789513519349.
[25] A.R. Torabi, F. Berto, Fracture assessment of blunt V-notched graphite specimens by means of the strain energy density, Strength Mater. 45 (2013) 635–647, http://dx.doi.org/10.1007/s11223-013-9500-z.
[26] A.R. Torabi, A. Campagnolo, F. Berto, Tensile fracture analysis of V-notches with end holes by means of the local energy, Phys. Mesomech. 18 (2015) 5–12.
[27] D. Radaj, State-of-the-art review on the local strain energy density concept and its relation to the *J* -integral and peak stress method, Fatigue Fract. Eng. Mater. Struct. 38 (2015) 2–28, http://dx.doi.org/10.1111/ffe.12231.
[28] F. Berto, P. Lazzarin, Recent developments in brittle and quasi-brittle failure assessment of engineering materials by means of local approaches, Mater. Sci. Eng. R Reports. 75 (2014) 1–48, http://dx.doi.org/10.1016/j.mser.2013.11.001.
[29] F. Berto, P. Lazzarin, A review of the volume-based strain energy density approach applied to V-notches and welded structures, Theor. Appl. Fract. Mech. 52 (2009) 183–194, http://dx.doi.org/10.1016/j.tafmec.2009.10.001.
[30] F. Berto, A. Campagnolo, P. Gallo, Brittle failure of graphite weakened by V-notches: a review of some recent results under different loading modes, Strength Mater. 47 (2015) 488–506, http://dx.doi.org/10.1007/s11223-015-9682-7.
[31] P. Gallo, T. Sumigawa, T. Kitamura, F. Berto, Evaluation of the strain energy density control volume for a nanoscale singular stress field, Fatigue Fract. Eng. Mater. Struct. 39 (2016) 1557–1564, http://dx.doi.org/10.1111/ffe.12468.
[32] Q. Sun, Q. Guo, X. Yao, L. Xiao, J.R. Greer, J. Sun, Size effects in strength and plasticity of single-crystalline titanium micropillars with prismatic slip orientation, Scr. Mater. 65 (2011) 473–476, http://dx.doi.org/10.1016/j.scriptamat.2011.05.033.
[33] D. Kiener, W. Grosinger, G. Dehm, R. Pippan, A further step towards an understanding of size-dependent crystal plasticity: in situ tension experiments of miniaturized single-crystal copper samples, Acta Mater. 56 (2008) 580–592, http://dx.doi.org/10.1016/j.actamat.2007.10.015.
[34] O. Kamigaito, Ideal fracture stress of brittle material having no defect, J. Mater. Sci. Lett. 7 (1988) 529–531, http://dx.doi.org/10.1007/BF01730717.
[35] D. Taylor, The Theory of Critical Distances: A New Perspective in Fracture Mechanics, first ed., Oxford, 2007.
[36] P. Gallo, Y. Yan, T. Sumigawa, T. Kitamura, Fracture behavior of nanoscale notched silicon beams investigated by the theory of critical distances, Adv. Theory Simulations. 1 (2018) 1700006, http://dx.doi.org/10.1002/adts.201700006.
[37] P. Lazzarin, F. Berto, M. Elices, J. Gómez, Brittle failures from U- and V-notches in mode I and mixed, I + II, mode: a synthesis based on the strain energy density averaged on finite-size volumes, Fatigue Fract. Eng. Mater. Struct. 32 (2009) 671–684, http://dx.doi.org/10.1111/j.1460-2695.2009.01373.x.
[38] Z. Yosibash, A. Bussiba, I. Gilad, Failure criteria for brittle elastic materials, Int. J. Fract. 125 (2004) 307–333.
[39] M.H. El Haddad, T.H. Topper, K.N. Smith, Prediction of non propagating cracks, Eng. Fract. Mech. 11 (1979) 573–584, http://dx.doi.org/10.1016/0013-7944(79)90081-X.
[40] P. Lazzarin, C.M. Sonsino, R. Zambardi, A notch stress intensity approach to assess the multiaxial fatigue strength of welded tube-to-flange joints subjected to combined loadings, Fatigue Fract. Eng. Mater. Struct. 27 (2004) 127–140, http://dx.doi.org/10.1111/j.1460-2695.2004.00733.x.
[41] P. Lazzarin, F. Berto, F.J. Gómez, M. Zappalorto, Some advantages derived from the use of the strain energy density over a control volume in fatigue strength assessments of welded joints, Int. J. Fatigue. 30 (2008) 1345–1357, http://dx.doi.org/10.1016/j.ijfatigue.2007.10.012.
[42] D. Taylor, The theory of critical distances, Eng. Fract. Mech. 75 (2008) 1696–1705, http://dx.doi.org/10.1016/j.engfracmech.2007.04.007.
[43] L. Susmel, D. Taylor, The theory of critical distances as an alternative experimental strategy for the determination of KIc and ΔKth, Eng. Fract. Mech. 77 (2010) 1492–1501, http://dx.doi.org/10.1016/j.engfracmech.2010.04.016.
[44] L. Susmel, D. Taylor, On the use of the Theory of Critical Distances to predict static failures in ductile metallic materials containing different geometrical features, Eng. Fract. Mech. 75 (2008) 4410–4421, http://dx.doi.org/10.1016/j.engfracmech.2008.04.018.
[45] J.J. Wortman, R.A. Evans, Young's modulus, shear modulus, and poisson's ratio in silicon and germanium, J. Appl. Phys. 36 (1965) 153–156, http://dx.doi.org/10.1063/1.1713863.
[46] E. Mandenci, I. Guven, The Finite Element Method and Applications in Engineering using ANSYS, Springer, 2006.
[47] P. Lazzarin, F. Berto, M. Zappalorto, Rapid calculations of notch stress intensity factors based on averaged strain energy density from coarse meshes: theoretical bases and applications, Int. J. Fatigue. 32 (2010) 1559–1567, http://dx.doi.org/10.1016/j.ijfatigue.2010.02.017.
[48] D. Taylor, The Theory of Critical Distances: a link to micromechanisms, Theor. Appl. Fract. Mech. 90 (2017) 228–233, http://dx.doi.org/10.1016/j.tafmec.2017.05.018.
[49] P. Cornetti, N. Pugno, A. Carpinteri, D. Taylor, Finite fracture mechanics: a coupled stress and energy failure criterion, Eng. Fract. Mech. 73 (2006) 2021–2033, http://dx.doi.org/10.1016/j.engfracmech.2006.03.010.
[50] F. Berto, P. Lazzarin, M.R. Ayatollahi, Brittle fracture of sharp and blunt V-notches in isostatic graphite under pure compression loading, Carbon N. Y. 63 (2013) 101–116, http://dx.doi.org/10.1016/j.carbon.2013.06.045.
[51] D.A. Cendón, A.R. Torabi, M. Elices, Fracture assessment of graphite V-notched and U-notched specimens by using the cohesive crack model, Fatigue Fract. Eng. Mater. Struct. 38 (2015) 563–573, http://dx.doi.org/10.1111/ffe.12264.
[52] P. Cornetti, A. Sapora, A. Carpinteri, Short cracks and V-notches: finite fracture mechanics vs. cohesive crack model, Eng. Fract. Mech. 168 (2016) 2–12, http://dx.doi.org/10.1016/j.engfracmech.2015.12.016.
[53] A.R. Torabi, S. Etesam, A. Sapora, P. Cornetti, Size effects on brittle fracture of Brazilian disk samples containing a circular hole, Eng. Fract. Mech. 186 (2017) 496–503, http://dx.doi.org/10.1016/j.engfracmech.2017.11.008.
[54] P. Weißgraeber, D. Leguillon, W. Becker, A review of finite fracture mechanics: crack initiation at singular and non-singular stress raisers, Arch. Appl. Mech. 86 (2016) 375–401, http://dx.doi.org/10.1007/s00419-015-1091-7.
[55] A. Sapora, A.R. Torabi, S. Etesam, P. Cornetti, Finite Fracture Mechanics crack initiation from a circular hole, Fatigue Fract. Eng. Mater. Struct. (2018), http://dx.doi.org/10.1111/ffe.12801.